Article

High-throughput, label-free isolation of white blood cells from whole blood using parallel spiral microchannels with U-shaped cross-section

Amirhossein Mehran[1], Peyman Rostami[1], Mohammad Said Saidi[1], Bahar Firoozabadi[1,*], Navid Kashaninejad[2,*]

[1] School of Mechanical Engineering, Sharif University of Technology, Tehran 11155, Iran; amirhossein.mehran@alum.sharif.edu (A.M.); peyman.rostami@mech.sharif.ir (P.R.); mssaidi@sharif.edu (M.S.S.); firoozabadi@sharif.edu (B.F.)

[2] Queensland Micro- and Nanotechnology Centre, Nathan Campus, Griffith University,170 Kessels Road, Brisbane, QLD 4111, Australia; n.kashaninejad@griffith.edu.au (N.K.)

* Correspondence: firoozabadi@sharif.edu (B.F.) and n.kashaninejad@griffith.edu.au (N.K.). Tel.: +61 7373 55391 (N.K.)

Abstract: Rapid isolation of white blood cells (WBCs) from whole blood is an essential part of any WBC examination platform. However, most conventional cell separation techniques are labor-intensive and low throughput, require large volumes of samples, need extensive cell manipulation, and have low purity. To address these challenges, we report the design and fabrication of a passive, label-free microfluidic device with a unique U-shaped cross-section to separate WBCs from whole blood using hydrodynamic forces that exist in a microchannel with curvilinear geometry. It is shown that the spiral microchannel with a U-shaped cross-section concentrates larger blood cells (e.g., WBCs) in the inner cross-section of the microchannel by moving smaller blood cells (e.g., red blood cells (RBCs) and platelets) to the outer microchannel section and preventing them from returning to the inner microchannel section. Therefore, it overcomes the major limitation of a rectangular cross-section where secondary Dean vortices constantly enforce particles throughout the entire cross-section and decrease its isolation efficiency. Under optimal settings, more than 95% of WBCs can be isolated from whole blood under high-throughput (6 ml/min), high-purity (88%), and high-capacity (180 ml of sample in 1 hour) conditions. High efficiency, fast processing time, and non-invasive WBC isolation from large blood samples without centrifugation, RBC lysis, cell biomarkers, and chemical pre-treatments make this method an ideal choice for downstream cell study platforms.

Keywords: WBC isolation, Spiral microchannels, Inertial microfluidics, Passive cell separation, High-throughput separation.

1. Introduction

In medical science, the study of characteristics and mechanisms of cell functions, identifying external damaging factors, and finding methods to prevent and treat cellular disorder diseases in the human body requires the preparation of cell samples with suitable purity. Blood is the most important component of the human body, containing various types of essential cells, including red blood cells (RBCs), white blood cells (WBCs), and platelets which are produced in the bone marrow and released into the bloodstream [1]. WBCs comprise about 1% of whole blood and have a significant role in the body's immune system. The change in the total number of WBCs in the blood is the harbinger of infections, autoimmune reactions, and other malignancies [2]. For example, in blood cancer diseases, such as leukemia and myeloma, the life cycle of normal blood cells is interrupted by the abnormal growth in the number of WBCs in the bone marrow and bloodstream. Hence, enumeration and monitoring of WBCs are critical in diagnosing various kinds of diseases [3]. Since RBCs comprise the majority of whole blood, complete or fractional separation of RBCs from a blood sample is usually required for subsequent cellular and molecular

Preprints (www.preprints.org) | NOT PEER-REVIEWED | Posted: 29 September 2021 doi:10.20944/preprints202109.0482.v1

examination of WBCs. However, conventional cell sorting techniques, such as density gradient centrifugation, RBC lysis, porous filteration, and other methods are often labor-intensive, require a large volume of sample, and sometimes use expensive particular biomarkers or labels to identify the target cells [4].

In recent years, various microfluidic cell separation devices have been developed to minimize the amount of required sample, processing time, and operator-based errors while maintaining high-throughput and isolation efficiency [5,6]. Although they have been successful, there is always a trade-off between the efficiency and throughput of these platforms. Based on the separation mechanism, microfluidic cell isolation techniques can be categorized into active and passive methods [6].

Active methods require an externally applied force so that cells are separated due to their different optical [7], electrical [8], or magnetic [9] properties. Some examples of the active methods are dielectrophoresis (DEP) [10], acoustophoresis [11] and magnetophoresis [12]. Although active methods have been proven to be useful in various biological applications, the low-throughput, complex mechanism, and high fabrication costs have limited their widespread applications in most cases.

Passive methods rely on label-free separation of cells using their physical properties without any externally applied force field. Some passive separation methods include deterministic lateral displacement (DLD) [13], pinch flow fractionation (PFF) [14], hydrodynamic filtration [15] and inertial migration [16].

Among passive cell separation techniques, inertial microfluidics has attracted much attention in recent years. The efficiency of inertial microfluidic for cell separation depends on inertial migration and hydrodynamic forces. Inertial migration is a function of the geometrical parameters of the device, while hydrodynamic forces separate particles based on their physical properties, such as density [17], size [18], or deformability [19].

Segre and Silberberg [20,21] were the first to report the inertial migration effect by showing that randomly incoming dispersed particles in a circular tube with a radius of R, can laterally migrate towards the channel walls and form a ring-shaped annulus with a radius of 0.6 R at the outlet. This observation led many researchers to investigate the physics of this phenomenon [22,23]. Particle lateral migration is affected by the shear gradient lift force, which moves the particles towards the tube walls. The wall induces lift force that pushes the particles through the tube centerline and prevents them from getting close to the walls. As a result, particles reach a certain equilibrium position in the tube's cross-section depending on the magnitude of these forces, flow velocity, and particle's physical properties [24]. Due to difficulties with particle separation at the outlet of a circular tube, several studies have investigated particle's inertial migration in non-circular channels [25-27]. In a square microchannel, eight stable particle equilibrium positions (corners and midline of channel edge) exist in relatively low Reynolds number flows ($Re < 100$) [25]. However, increasing the Reynolds number ($Re > 500$) will reduce the equilibrium positions to four, in which particles are focused at microchannel corners [25]. In a straight rectangular microchannel, randomly dispersed particles with $a_p/D_h \sim 0.1$ (where a_p is particle diameter and D_h is hydraulic diameter of the channel) align in four equilibrium positions where shear gradient lift force and wall induced lift force balance each other [27]. According to recent studies, in a spiral microchannel, particles are focused in one single equilibrium position close to the inner wall of the microchannel while smaller sized particles continue to recirculate by the effect of the secondary Dean flow [16,28].

Recently, many studies have been performed to optimize separation by increasing throughput, separation efficiency, and resolution in a spiral microchannel [29,30]. Some studies developed numerical calculations to better understand the inertial focusing mechanism [31,32]. Some studies have been investigated to modify microchip geometry to optimize the flow rate and isolation efficiency. Label-free tumor cell separation from whole blood has been conducted using a double spiral microchannel device with 88.5% tumor recovery rate as well as 92.28% recovery for blood cells [33]. Higher particle isolation efficiency was reached by introducing a spiral microchannel with trapezoidal cross-section [34,35] and ordered micro-obstacles [36]. However, the complex fabrication of and

Preprints (www.preprints.org) | NOT PEER-REVIEWED | Posted: 29 September 2021 doi:10.20944/preprints202109.0482.v1

trapezoidal cross-section and micro-obstacles has limited the wide application of this kind of geometry in microfluidic platforms. Our group proposed a spiral microchannel with a stair-like cross-section for size-based particle separation. Using equilibrated vortices present in the spiral microchannel, it was observed that there is a size-dependent threshold for flow rate for separating each specific particle [37].

This work overcomes the limitations of previous methods by presenting a passive microfluidic approach for high-throughput continuous isolation of WBCs from whole blood in a spiral microchannel with a U-shape cross-section using size-dependent inertial migration. The proposed method uses secondary Dean drag force to move smaller cells away and inertial forces to equilibrate larger cells through the spiral microchannel. One of the advantages of the U-shape cross-section is that target cells can be collected from separate outlets in discrete cell streams without any restriction on channel length. The U-shaped cross-section also avoids the re-circulation of smaller particles through the entire cross-section. Hence, it removes certain drops in isolation efficiency due to the mixing problems of conventional rectangular cross-sections. Unlike previous methods, the proposed spiral microchannels with the U-shaped cross-section are easy to fabricate. Also, we have developed a novel numerical algorithm to calculate inertial migration forces exerted on particles to optimize the proposed device's cell separation capability that can be used for similar inertial focusing methods for future works. It also further eliminates the time-consuming process of trial and error to find the optimized design of the device. Based on numerical results, we select an optimized geometry regarding the proper placement of the secondary vortices and their primary role in carrying the target cells to proper microchip outlets. Utilizing this method, high separation efficiency for WBCs and high removing ratios for RBCs and platelets were achieved using the fabricated parallel spiral microchannels with a U-shaped cross-section. It was reached under a high-throughput (as high as 6 ml/min), high-capacity (360 ml sample in 1 hour) label-free cell sorting without the need for any significant pre-processing or post-processing. Single-layer spiral microchannel with the U-shaped cross-section, which is a modified version of a spiral microchannel with rectangular cross-section, has the following advantages: i) Strong commercialization potentials due to simplified fabrication methods; ii) Low fabrication costs and efforts; iii) A wide-range separation of cells/particles with different sizes. Such an optimized microfluidic device has great potential for biological cell separation in clinical applications.

2. Design principle

In straight channels, shear-induced lift force resulting from the parabolic nature of the velocity profile in a Poiseuille flow tends to move the dispersed particles away from the center of the microchannel towards the channel walls. As the particle gets closer to the walls, an asymmetric wake around the particle forms a wall-induced lift force that prevents the particles from getting close to the walls and directs them away from the walls to the channel center [38]. Hence, the particles reach equilibrium positions in narrow bands where these two opposite forces are equal [20,21,25,28,39,40]. The overall magnitude of inertial forces which cause the lateral migration of the particles in a straight microchannel can be estimated by Eq. 1 [41]:

$$F_L = \rho G^2 C_L(Re, x_p)\, {a_p}^4 \tag{1}$$

where ρ is the density of the fluid, G is the fluid shear rate ($G = 2U_f/D_h$), U_f is the average flow velocity, C_L is a non-dimensional lift coefficient which is a function of Reynolds number and particle position in the channel's cross-section, U is the maximum velocity in the microchannel, D_h is the hydraulic diameter of the microchannel and a_p is the particle diameter. The magnitude of C_L and thus F_L starts from zero in the channel centerline, reaches a maximum value, and then goes back to zero again around $0.2D_h$ away from the channel wall, which is considered as the equilibrium position of particles [41]. Beyond

Preprints (www.preprints.org) | NOT PEER-REVIEWED | Posted: 29 September 2021 doi:10.20944/preprints202109.0482.v1

this distance, C_L becomes negative in sign showing the dominance effect of wall-induced lift force and further increases in magnitude by moving towards the walls [27].

Fluid flow in curvilinear channels experiences radially outward centrifugal acceleration resulting in the shift of maximum velocity towards the outer wall of the channel, leading to the formation of two counter-rotating vortices known as Dean vortices in the top and bottom halves of the channel cross-section plane [42,43]. The strength of these two identical vortices can be described using the dimensionless Dean number (De):

$$De = \frac{\rho U_f D_h}{\mu} \sqrt{\frac{D_h}{2R}} = Re \sqrt{\frac{D_h}{2R}} \quad (2)$$

where ρ is the fluid density, U_f is the average flow velocity, μ is the fluid viscosity, D_h is the hydraulic diameter, R is the flow path curvature, and Re is the flow Reynolds number. Assuming Stokes law, particles are affected by the drag force due to the presence of the secondary flow in the microchannel, which can be described as:

$$F_D = 3\pi\mu\, U_{Dean} \quad (3)$$

where μ is the fluid viscosity and a_p is the particle diameter. U_{Dean} is the average Dean velocity and is formulated by Ookawara *et al.* [44,45]:

$$U_{Dean} = 1.8 \times 10^{-4}\, De^{1.63} \quad (4)$$

Thus, the drag force caused by secondary Dean vortices exerted on the particles can be estimated by:

$$F_D = 5.4 \times 10^{-4}\, \pi\mu\, De^{1.63}\, a_p \quad (5)$$

Inertial forces and Dean drag forces act in the same direction on the particles near the outer wall while particles near the inner wall experience these two forces in opposite directions. According to Equations (1) and (5), the ratio of inertial lift force to Dean drag force (F_L/F_D) is proportional to $a_p{}^3$, therefore, as particles become larger, the inertial lift force exerted on them becomes greater than Dean drag force and vice versa for small particles. Hence, in a spiral microchannel, larger particles tend to reach equilibrium near the inner wall of the channel, while smaller ones are circulated constantly by the secondary flow.

In this paper, we take advantage of the simultaneous acting of inertial forces and Dean drag force on the blood cells in a spiral microchannel to develop a high-throughput device that can isolate WBCs from whole blood without the needs of blood lysis, cell labeling, centrifugation, and other chemical or physical pre-processing techniques on the sample.

3. Materials and methods

3.1. Device fabrication

The master mold was manufactured by micro-milling on a PMMA (polymethyl methacrylate) by Dahlih MCV-1020A Milling Machine. The chip was fabricated using the standard soft lithography method. Briefly, degassed PDMS (polydimethylsiloxane), mixed in a 10:1 pre-polymer base to the curing agent, was cast onto the master mold and baked in a vacuum oven for 4 hours at 75°C. Cured PDMS layer with embedded channels was peeled off, and inlets and outlets holes were punched using a 2 mm biopsy punch. The final microchip on PDMS was irreversibly bonded to a thick standard glass slab with an oxygen plasma and subsequently baked for 2 hours at 85 ℃ to further improve the bonding. Silicone tubes with an outer diameter of 2 mm were press-fitted into the channel inlets and outlets. The device consists of two parallel 4-loop spiral geometry with 4 inlets,

Preprints (www.preprints.org) | NOT PEER-REVIEWED | Posted: 29 September 2021 doi:10.20944/preprints202109.0482.v1

and 2 shared inner and outer outlets for each spiral. The cross-section of the channels is a U-shape geometry with 700 μm width and 200 μm height, and the two sections of the channel are connected by a 200 μm × 80 μm passway as shown in **Error! Reference source not found.**B.

Each spiral microchannel has an initial radius of curvature of 6 mm and a distance of 1.9 mm between two successive loops. The total length of each spiral channel is approximately 17.6 cm (**Error! Reference source not found.**A).

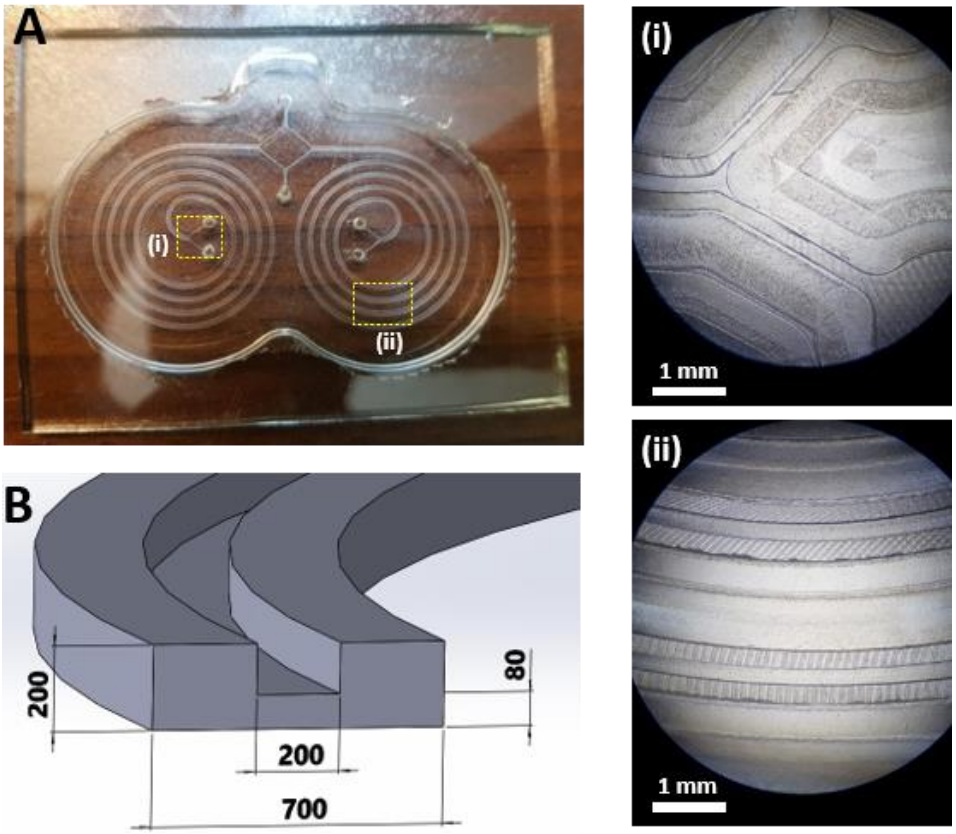

Figure 1. A) The 4-loop parallel spiral microchannel fabricated in PDMS with the corresponding mold preview. (i) The magnified view of section (i). (ii) The magnified view of section (ii). B) Schematic of the cross-section of the spiral microchannel. The dimensions are in μm.

3.2. Numerical simulation

The main idea of simulation is to calculate the forces exerted on the cells in the fluid domain. Since the cells' size is relatively comparable to microchannel dimensions (14 μm vs. 200 μm), the effect of cells on the fluid domain cannot be ignored. Di Carlo et al. [31] developed an algorithm to calculate the inertial forces exerted on particles in a straight rectangular microchannel. A modified version of this algorithm is developed for a complex U-shaped cross-sections microchannel in the present work.

Inertial lift force is a function of particle location within the cross-section of a microchannel and flow shear rate around the particle. We aim to calculate this force within the cross-section and investigate the equilibrium positions of particles through the cross-section plane. The simulation consists of three steps:

a) A 3D steady laminar flow is solved through the whole spiral microchannel, and velocity profiles are extracted using COMSOL Multiphysics® software.

b) A straight channel with a proposed cross-section with a length of 20 times the particle diameter is created.

The velocity profile solved at Step (a) is set as the inlet and outlet boundary conditions, and the flow field is calculated through the entire P-channel. Linear and rotational velocities of flow on some cross-section points will be used in the next step.

Preprints (www.preprints.org) | NOT PEER-REVIEWED | Posted: 29 September 2021 doi:10.20944/preprints202109.0482.v1

c) Particle modeled as a solid sphere is put in the middle of the microchannel alongside the x-direction, and its location is set to change in *zy* plane in each solution step. Steady-state linear and rotational velocities of the particle are unknown and should be calculated using an iterative trial-and-error process.

The flowchart of the proposed algorithm is shown in **Error! Reference source not found.**.

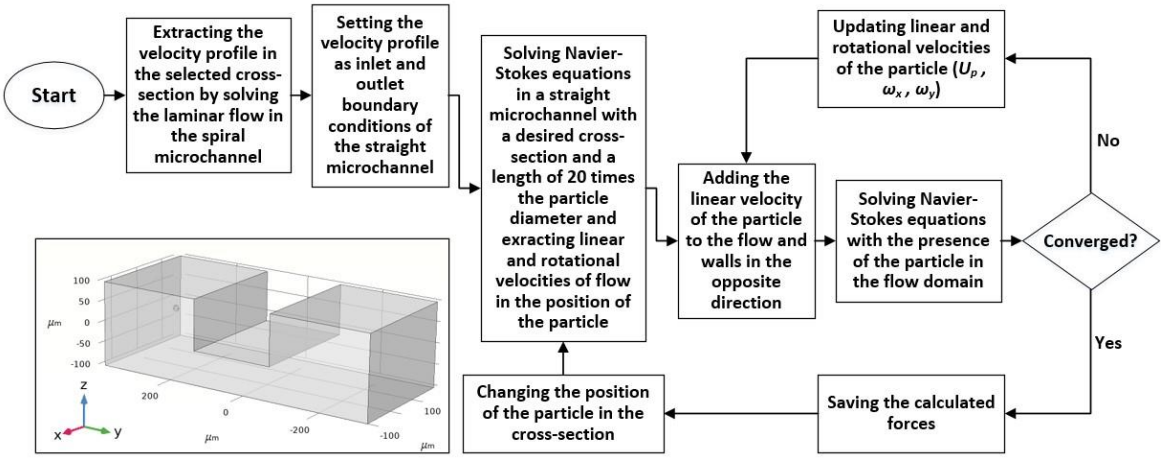

Figure 1. Flowchart of the numerical algorithm used in this study for the calculation of the forces exerted on particles. The original algorithm was presented to investigate particle's inertial migration in a straight microchannel [28]. Such an algorithm was later modified to be used in a rectangular spiral microchannel [32]. We extended the original algorithm to be capable of calculating any other desired microchannel cross-sections.

The governing equations for fluid flow within the microchannel are continuity and Navier-Stokes equations as follows [46,47]:

$$\rho \nabla . u = 0 \tag{6}$$

$$\rho(\boldsymbol{u}.\nabla)\boldsymbol{u} = \nabla.[-p\boldsymbol{I} + \mu(\nabla\boldsymbol{u} + (\nabla\boldsymbol{u})^T)] \tag{7}$$

where ρ is the fluid density, ∇ is the differential (Del) operator, $\boldsymbol{u}$ is the flow velocity vector, $\boldsymbol{I}$ is the identity tensor and p is the pressure. Navier-Stokes equations are solved using the finite element method and P2+P2 scheme is chosen to discretize the velocity and pressure.

In order to start the algorithm (Step c), we set the initial linear and rotational velocity of the particle equal to the fluid velocities at the exact location of the particle, which was solved in Step (b). In fact, these initially estimated velocities are from the case in which no particle is present in the flow field.

Moving wall boundary condition is applied to channel walls with velocities equal to particle's linear velocity (U_p) in the opposite direction (-x):

$$U_{wall} = -U_p \tag{8}$$

Channel inlet and outlet are set to the same velocity profile given in Step (b) and are updated in every iteration using the particle's axial velocity as follows:

$$U_{in} = U_{fluid,old} - U_p \tag{9}$$

Particle is treated as a solid sphere with rotating walls:

$$\vec{U} = \overrightarrow{\Omega_p} \times \left(\vec{r} - \vec{r_p}\right) \tag{10}$$

Preprints (www.preprints.org) | NOT PEER-REVIEWED | Posted: 29 September 2021 doi:10.20944/preprints202109.0482.v1

where $(\vec{r} - \vec{r_p})$ represents the location of a point on particle surface relative to its center with a flow velocity vector of $\vec{U}$, and $\overrightarrow{\Omega_p}$ represents the particle rotational velocity vector.

Particle rotational and axial linear velocities are updated during the calculations until the axial force, and cross-sectional components of momentum exerting on the particle become less than 1×10^{-14} N and 1×10^{-20} N.m, respectively, hence, to be considered as a steady-state condition for the particle. Once convergence occurs, calculations will start over with the particle being placed at another location in the zy plane. The following formulas are used to update the velocities:

$$U_p'' = U_p' + a_z \times \Delta t \tag{11}$$

$$\Omega_x'' = \Omega_x' + \alpha_x \times \Delta t \tag{12}$$

$$\Omega_z'' = \Omega_z' + \alpha_z \times \Delta t \tag{13}$$

where superscripts indices ($''$) and ($'$) respectively refer to old and new calculated parameters, U_p is the axial linear velocity of the particle, and a_x, α_y and α_z are the linear and cross-sectional rotational accelerations of the particle, respectively which can be found using the Newton's second law of motion.

After the inertial forces are calculated for a specific particle in the whole cross-section, we can investigate whether the particle can be moved through the middle passway by the secondary flow field or not, hence characterizing the ability of the microchannel to separate the target cells.

3.3. Mesh independency

A mixed structured-unstructured type of mesh was used with the presence of the particle in the microchannel (**Error! Reference source not found.**). The microchannel was split into two distinct parts: i) a block containing the particle with a cross-section similar to the cross-section of the channel in which triangular and tetrahedral grids were used for the surface of the particle and the rest of the zone, respectively, ii) other zones excluding the particle in which structured grids were used. The inertial lift force exerted on the particle in the y-direction throughout the microchannel cross-section was selected as the mesh independency criteria and various mesh resolutions were considered to evaluate grid independency. The results show that the maximum value for different parameters, including the width of the block containing the particle, size of the tetrahedral grids, and size of the triangular grids on the surface of the particle are $5\times D_p$, $0.1\times D_p$, and $0.05\times D_p$, respectively, in order to preserve less than 0.1% change in the y-component of the lift force with D_p being the particle diameter.

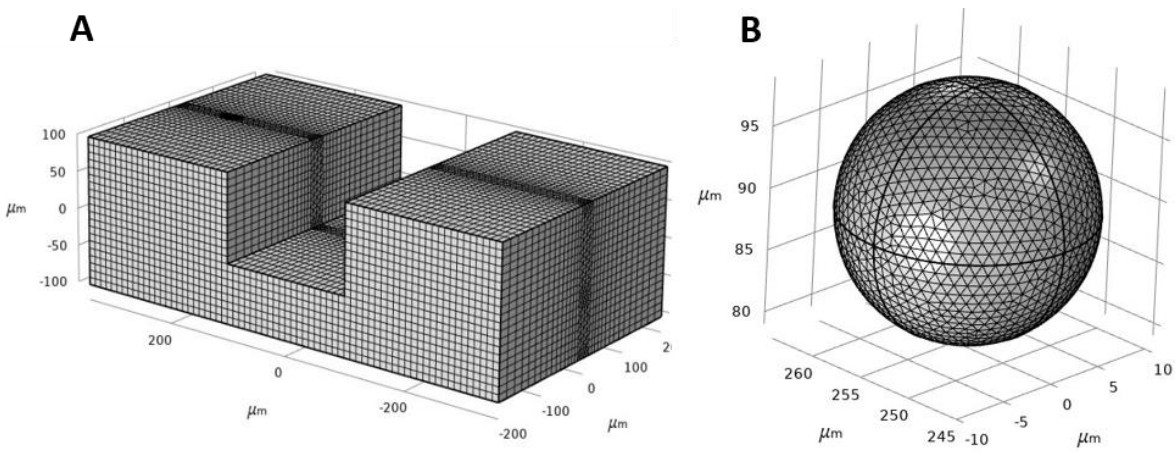

Preprints (www.preprints.org) | NOT PEER-REVIEWED | Posted: 29 September 2021 doi:10.20944/preprints202109.0482.v1

Figure 3. Illustration of the mesh in the fluid domain. A) The domain was separated into two zones in which tetrahedral mesh was used between the particle surface and the microchannel walls with a maximum size of 0.1× D_p, and the structured mesh was used outside the block, including the particle. B) Triangular mesh was used on the surface of the particle with a maximum size of 0.05× D_p.

3.4. Sample preparation

Blood samples were collected using a blood collection tube. 10 ml of blood was mixed with 35 µL ethylenediaminetetraacetic acid (EDTA) solution (7 µL per 2 ml of blood) to prevent blood clotting. The study was approved by the Research Ethics Committees of Iran University of Medical Sciences (ID: IR.IUMS.REC.1400.285), and the subject was given written informed consent. In addition, all clinical experiments were conducted in accordance with the ethical principles and related guidelines. Due to non-Newtonian behavior and high concentration of RBCs in the blood, we diluted the whole blood with DI water. Three tubes of the sample were prepared by mixing the whole blood with DI water with the ratios of 1:9, 1:22.5, and 1:45, yielding blood samples with 1%, 2%, and 5% hematocrit, respectively.

3.5. Experimental approach

Throughout the tests, prepared blood samples were pumped through the spiral's inner inlet into the chip using a 10 ml syringe on a syringe pump with flows varying from 2 ml/min up to 8 ml/min and equal flow of DI water as sheath flow to the outer inlet. Processed samples were collected from inner and outer outlets in silicone tubes, and cell counting was done using a Neubauer chamber. The ratio of WBCs in the inner outlet to the whole WBC cells in both outlets samples is reported as WBC isolation efficiency of the spiral microchannel:

$$\%WBC = \frac{\#\ of\ WBC\ in\ the\ inner\ outlet}{\#\ of\ WBC\ in\ (inner + outer)\ outlets} \tag{14}$$

Moreover, the removing ratio of RBCs and platelets are obtained using the equations below:

$$\%RBC = \frac{\#\ of\ RBC\ in\ the\ outer\ outlet}{\#\ of\ RBC\ in\ (inner + outer)\ outlets} \tag{15}$$

$$\%Platelets = \frac{\#\ of\ Platelets\ in\ the\ outer\ outlet}{\#\ of\ Platelet\ in\ (inner + outer)\ outlets} \tag{16}$$

In order to get well-balanced results, DI water was set to be pumped into the spiral microchannel to wash it out from the remaining blood cells from previous use before running further tests.

4. Results and discussion

4.1. Device design for cell separation

The concept of cell separation in this method is illustrated in Figure 2. The U-shaped cross-section design proposed in this study can keep large particles, such as WBCs, in the inner microchannel section, while forcing smaller cells, like RBCs and platelets, to migrate to the outer microchannel section through the middle pass way without recirculating and coming back to the inner section of the microchannel. Accordingly, the proposed U-shaped cross-section eliminates the re-circulation and mixing problems of conventional rectangular cross-sections. In order to reach a decent isolation flow rate, two identical spiral microchannels are set as parallel to each other, with inner outlets and outer outlets being merged into a single inner and outer outlet, respectively. At the end of the experiment, WBCs ($a_p \sim 14\ \mu m$) are collected from the inner outlets and RBCs ($a_p \sim 7\ \mu m$) and platelets ($a_p \sim 3\ \mu m$) are collected from outer outlets. Due to the size and flow dependence of the forces exerting on the blood cells, we manage to investigate the effect of flow

Preprints (www.preprints.org) | NOT PEER-REVIEWED | Posted: 29 September 2021 doi:10.20944/preprints202109.0482.v1

rate and cell concentration on the isolation efficiency in the spiral microchannel to find the optimum flow rate.

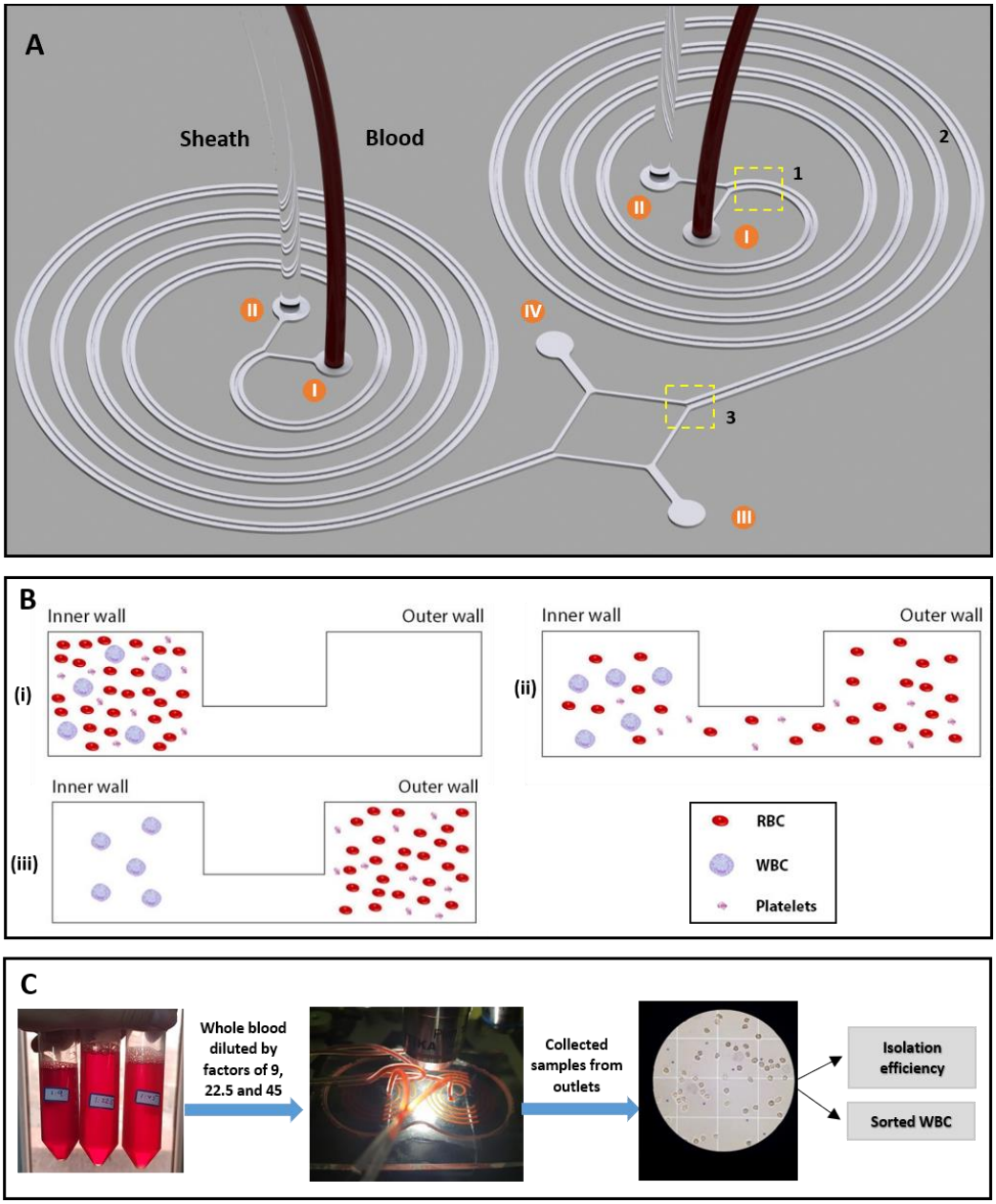

Figure 2. (A) 3D schematics of the proposed spiral microchip in this study. The design including two parallel U-shaped cross-section spiral microchannel that consists of: I) two inner inlets for the injection of blood samples, II) two outer inlets for the injection of sheath fluid, III) shared outer outlet for the extraction of RBC and platelets and IV) shared inner for the extraction of WBC. (B) Larger blood cells, i.e., WBC, affected by dominant inertial forces are focused along the inner microchannel wall. In comparison, smaller blood cells, i.e., RBC and platelets, are forced to migrate towards the outer microchannel section by the effect of the secondary flow (flow direction is shown in green arrows), which in turn stops the smaller cells from getting back to the inner microchannel section. (C) The overall process of WBC sorting and enumeration. Blood cell count is done using a Neubauer chamber, and the resulting blood cell efficiency is calculated using the fractional ratio of blood cells in specific outlets to the total count of blood cells in both outlets.

4.2. Validation of the numerical simulations

The microfluidic device proposed by Di Carlo et al. [31] was a straight channel with 50 μm × 40 μm rectangular cross-section, and the diameter of the particle was 10 μm in a flow with *Re=80*. In order to validate our algorithm, inertial lift forces acting on a 10 μm

Preprints (www.preprints.org) | NOT PEER-REVIEWED | Posted: 29 September 2021 doi:10.20944/preprints202109.0482.v1

particle are calculated in the same straight microchannel (Figure 3A). Particle equilibrium positions are located in the areas where the force vector approaches zero value, approximately 0.6 times of half channel width. As can be seen in Figure 3B, our simulations are quite consistent with Di Carlo's results [31] and demonstrate the same equilibrium regions. Next, we investigated the ability of the developed algorithm in this study by performing the calculations in the U-shaped cross-section microchannel.

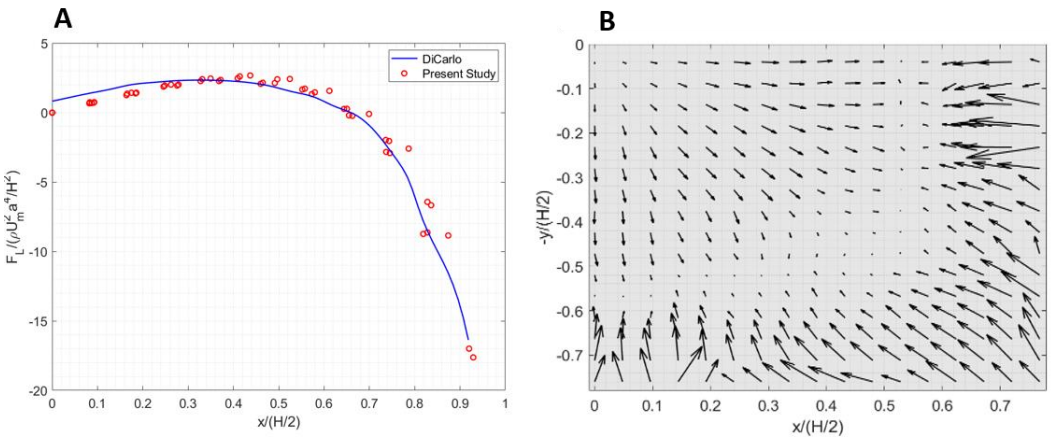

Figure 3. A) Calculated inertial force in a straight channel using the algorithm in the present study versus inertial force reported by Ref. [31]. B) Calculated inertial force field exerted on a 10 μm particle in the present study.

4.3. Simulation of the secondary flow in the spiral microchannel

In a conventional rectangular-cross-section spiral microchannel, pressure gradient results in the secondary flow formation consisting of two similar counter-rotating Dean vortices. However, in our geometry, secondary flow consists of four Dean vortices locating at the top and bottom of the inner and outer channel sections. Dean vortices' strength is increased by further increasing the flow rate and Dean number, and therefore, the vortex cores start to appear (Figure 4).

Preprints (www.preprints.org) | NOT PEER-REVIEWED | Posted: 29 September 2021 doi:10.20944/preprints202109.0482.v1

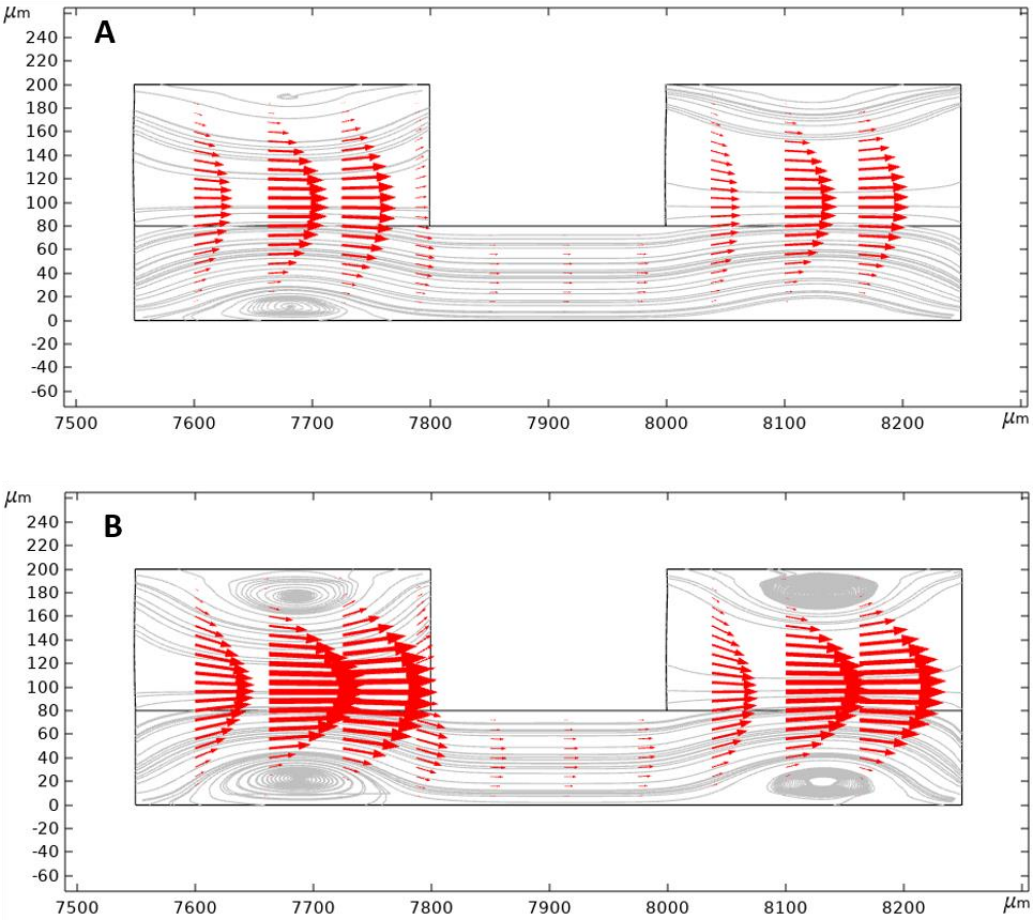

Figure 4. Calculated secondary flow streamlines and velocity vectors in the 2nd loop of the designed spiral microchannel cross-section. Velocity vectors are being directed from the inner wall to the outer wall in the middle passway with: A) 2 ml/min, B) 3 ml/min inlet flow rate.

Contours of velocity magnitude and the schematic of the flow velocity profile in this study are shown in

Figure 4A, B. As can be seen, there are two locations of maximum velocity in the inner and outer section of the microchannel, with the magnitude of maximum velocity in the inner section being higher than the outer one. This difference generates a pressure gradient that causes the secondary flow's streamline to be directed from the inner section towards the microchannel's outer section. Thus, the secondary flow keeps the migrated particles from returning to the inner microchannel section through the middle passway. This option removes the possibilities of cell circulation through the entire cross-section and increases the isolation efficiency.

The calculated inertial force field acting on a 10 μm particle in the U-shape channel is shown in Figure 5C. According to the simulation results, 10 μm particles migrate from the center of the microchannel's inner section towards the microchannel walls. As the particles get closer to the walls, a rather large inertial force stops them from further approaching the walls. The particles (can be removed) tend to reach equilibrium positions where the total amount of inertial forces exerting on them equals zero; these positions are shown as blue dashed lines.

The U-shape microchannel's capability to isolate the particles depends on the value of the exerted inertial forces and Dean drag force on the particles near the middle passway. Suppose the Dean drag force overcomes the inertial forces. In that case, the particles migrate to the outer microchannel section through the middle passway and, due to the direction of the streamlines, they cannot come back to the inner section. The inertial lift force profile exerted on a 10 μm particle alongside the y-direction is given in two different microchannel heights at the beginning of the middle passway in Figure 5D According to

Preprints (www.preprints.org) | NOT PEER-REVIEWED | Posted: 29 September 2021 doi:10.20944/preprints202109.0482.v1

the calculation results for 5 ml/min flowrate, the Dean drag force is strong enough to overcome the inertial forces exerting on particles smaller than 10 μm, hence moving them to the outer microchannel section. However, for particles larger than 10 μm, the inertial lift force near the passway walls is strong enough to overcome the dean drag force to keep these particles in the inner section. We did our calculations based on a 10 μm particle to ensure a safe particle diameter margin in which WBCs ~ 14 μm are isolated from smaller particles (RBCs ~ 7 μm and platelets ~ 3 μm) in the designed spiral microchannel. The optimum flow rate for the isolation of blood cells will be investigated through an experiment, which will be discussed in the next sections.

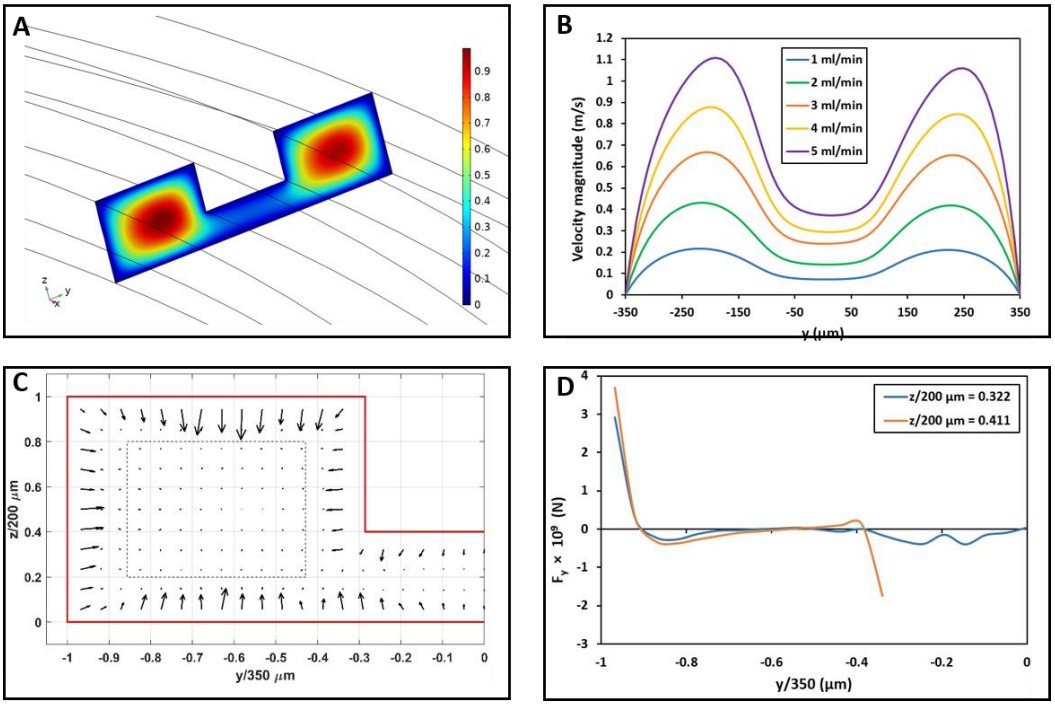

Figure 5. A) Contour of velocity magnitude (m/s) in the spiral microchannel at the second loop with the inlet flow rate of 3 ml/min. B) Velocity magnitude profile with the change in inlet flow rates at z=40 μm (z=0 indicates the bottom wall of the microchannel and y=0 indicates the middle of the microchannel cross-section), this difference in the maximum velocity magnitude results in the streamlines being directed from the inner microchannel wall towards the outer microchannel wall. C) The calculated inertial force field acting on a 10 μm particle in the spiral microchannel's inner section with the inlet flow rate of 5 ml/min. Equilibrium positions are shown as blue dashed lines in the microchannel cross-section. D) The inertial force exerted on a 10 μm particle alongside y-direction at z= 64.4 μm (z/200 μm = 0.322) and z= 82.2 μm (z/200 μm = 0.411). As can be seen, the inertial force at beginning of the passway is much lower than the wall-induced inertial force. The Dean drag force is able to overcome this inertial force, therefore, allowing the particles smaller than 10 μm to move toward the other section of the spiral microchannel.

4.4. Presence of the secondary flow in the spiral microchip

In order to confirm the presence of the secondary flow in the spiral microchannel, two syringes of fluid were prepared. One syringe was filled with colored fluid, while the other one was filled with DI water. The colored fluid was introduced into the spiral microchannels through the inner inlets, and DI water was set to enter through the outer inlets. The two syringes with 10 ml capacity were driven at 5 ml/min (2.5 ml/min per spiral) (*Re=81.7, De=11.2*) using a syringe pump, and images of the flow were captured at the inlets and outlets of the left side spiral microchannel (can be removed). As shown in **Figure 7**, the colored fluid filled the entire section of the microchannel at the outlet bifurcation, showing the Dean vortices' effect to mix the flow in both the inner and outer sections of the spiral microchannel.

Preprints (www.preprints.org) | NOT PEER-REVIEWED | Posted: 29 September 2021 doi:10.20944/preprints202109.0482.v1

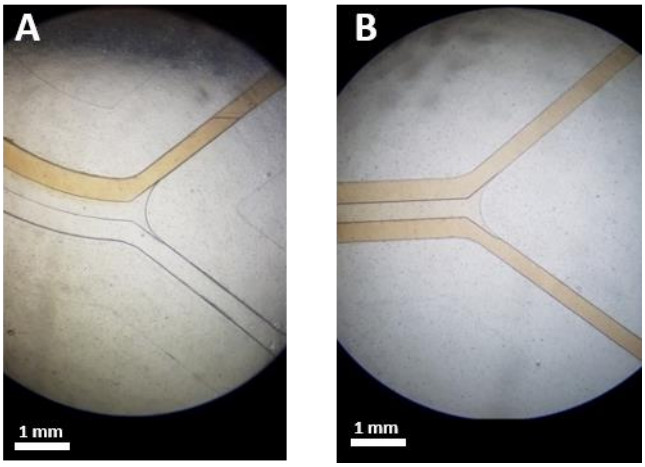

Figure 6. Images of the left side spiral microchannel at a) Inlets, b) outlets showing the effect of the secondary flow on mixing the colored fluid throughout the entire microchannel. The colored fluid and DI water were pumped through the microchannel from the inner and outer inlets, respectively.

4.5. The effect of the flow rate

To investigate the effect of flow rate on the separation of blood cells, a blood sample with a hematocrit of 1% was injected into the spiral microchannel through the inner inlets with 2-8 ml/min flowrate (with 1 ml/min step), and DI water was injected through the outer inlets as the sheath flow with the same flow rate. Multiple numbers of tests were done for each flow rate to reduce the uncertainty and errors caused by devices and cell enumeration.

As shown in Figure 7A, RBCs' removing ratio reaches a maximum value of 95.7% by increasing the blood sample flow rate up to 6 ml/min and then decreases with further flowrate increment.

The initial expectation would be that for sample flow rates higher than 6 ml/min, small cells do not have enough time (length) to migrate from the inner to outer section due to higher linear velocity. However, further investigations show that increasing the flow rate increases the inertial force more than the Dean drag force. The resultant force stops the majority of the red blood cells from migrating through the middle passway, and, hence, the overall efficiency decreases. Additionally, local perturbations in the place of outlet bifurcation negatively affect the isolation efficiency, which causes the particles to exit through the wrong outlets and further reducing the separation efficiency.

Unlike the RBCs and WBCs in which inertial and Dean drag forces exerting on them compete with each other all the time, platelets are always affected by Dean drag force due to their very small diameter. Removing ratio for platelets reaches a maximum value of 94.6% at a flow rate of 4 ml/min and remains almost constant up to 8 ml/min. Since inertial forces and Dean drag force are proportional to the 4th and 1st power of the particle diameter, respectively, the value of the inertial forces exerting on the platelets are negligible, and they accumulate in the outer section of the spiral microchannel with a high average removing ratio (Figure 7C).

Preprints (www.preprints.org) | NOT PEER-REVIEWED | Posted: 29 September 2021 doi:10.20944/preprints202109.0482.v1

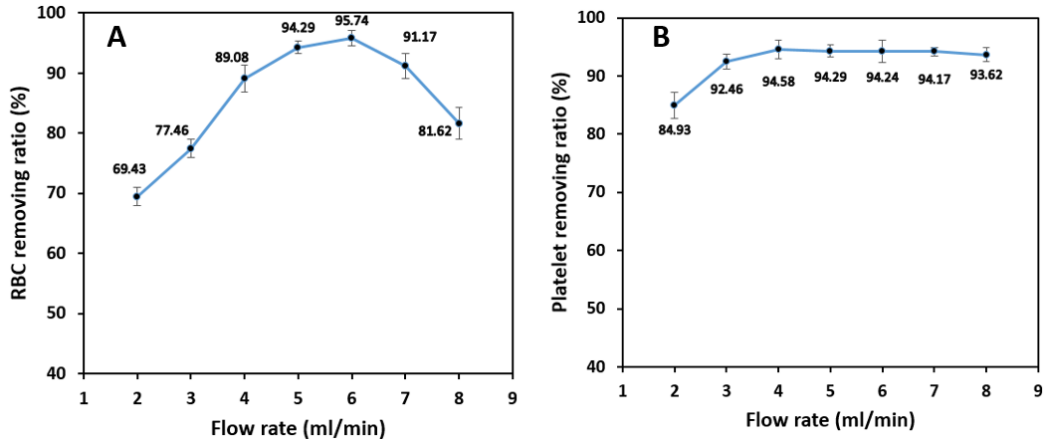

Figure 7. The effect of sample inlet flow rate on the removing ratio of A) RBC, B) Platelets for 1% blood hematocrit sample. RBC isolation efficiency is the most sensitive to changes in inlet flow rate with a maximum value at 6 ml/min. WBC isolation efficiency experiences a massive drop in higher flow rates due to the existence of high-strength dean vortices which force the WBCs to migrate to the outer microchannel wall. The isolation efficiency of platelets is the least dependent on the flow rate and they can be extracted from the shared outer outlets with high removing ratios.

Test results show that the isolation efficiency of WBCs from whole blood is almost stable up to a flow rate of 6 ml/min with 96.8% maximum efficiency at 5 ml/min. Increasing the sample flow rate has virtually no significant effect on the isolation of WBCs because the inertial forces have the leading role in keeping the cells in the inner section of a spiral microchannel. However, a further increase in flow rate from 6 ml/min increases the Dean vortices' strength, which tends to move the white blood cells to the outer section and decreases the WBCs isolation efficiency (Figure 8A). According to Figure 8B, WBC purity increases significantly from 44.3% at 2 ml/min to 88.3% at 6 ml/min by increasing the flow rate since the removing ratio of RBCs has also the same trend with respect to flow rate. A further increase in the flow rate results in a fall in purity since RBCs and platelets manage to remain in the inner section within the strong vortices.

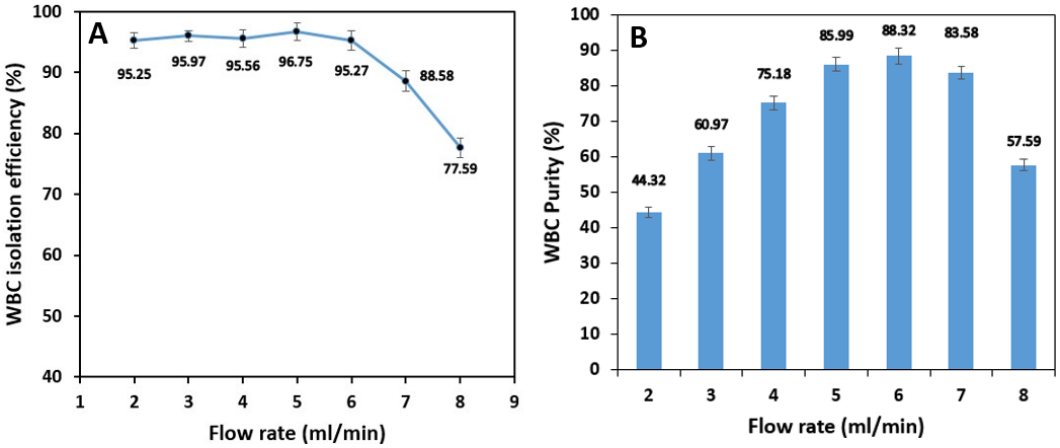

Figure 8. The effect of sample inlet flow rate hematocrit on WBCs': A) isolation efficiency, and B) purity for 1% blood hematocrit sample. The WBC isolation efficiency experiences a massive drop in higher flow rates due to the existence of high-strength dean vortices which force the WBCs to migrate to the outer microchannel wall. The outlet samples are the purest in flow rates of 4, 5, and 6 ml/min. The higher the removing ratio of RBCs and platelets, the higher WBC purity.

Since RBCs' removing ratio is highly dependent on the inlet flow rate, the overall criteria of the success of the spiral microchip on isolating the WBCs from whole blood must be selected based on the best isolation efficiency of WBCs and removing ratio of RBCs at the same time. As a result, for a 1% hematocrit blood sample, our spiral microchip can isolate WBCs from whole blood with 96.8% efficiency at the inlet flow rate of 6 ml/min

Preprints (www.preprints.org) | NOT PEER-REVIEWED | Posted: 29 September 2021 doi:10.20944/preprints202109.0482.v1

with a WBC sample purity of 88.3%. Moreover, the removing ratio of RBCs and platelets, in this case, are 95.8% and 94.2%, respectively.

Using flow rates of more than 8 ml/min is not applicable due to cell damage possibilities. Additionally, higher flow rates may break up the PDMS-glass slide bonding and are dangerous for test operators, so continuing the tests with flow rates of more than 8 ml/min was not possible.

4.6. The effect of hematocrit

The same methods and tests were applied on blood samples with 2% and 5% hematocrit to find the effect of the hematocrit on the efficiency of cell separation.

As shown in Figure 9A, the general trend of the removing ratio of RBCs remains the same for three tested blood hematocrits. Starting with relatively low values for 2 ml/min flow rate, removing ratio peaks at values of 88.4% and 82.5% by increasing the flow rate to 4 ml/min and 5 ml/min flow rates for 2% and 5% hematocrit, respectively, which is considered as a significant drop in isolation efficiency compared with 95.7% of 1% hematocrit blood sample. At relatively low flow rates, the difference in isolation efficiency is negligible for three hematocrits. However, in the 3-7 ml/min flow rate band, the ratio drops with the increase in hematocrit, and this difference tends to grow by increasing the flow rate. A decrease in removing ratio with an increase in hematocrit is due to the higher concentration of RBCs in higher blood hematocrits that raise the effect of cell-cell interaction force alongside the inertial forces and Dean drag force, which further degrades the overall removing ratio. Platelets typically focus on the outer microchannel section and can be extracted from the outer outlet at relatively high removing ratios. The effect of hematocrit on the isolation is relatively low in this case. It peaks at a value of 93.8% at 5 ml/min and 91.6% at 4 ml/min for 2% and 5% blood hematocrit, respectively, which is pretty much close to 94.2% extraction at 6 ml/min for 1% blood hematocrit. The reason is that the platelets are quite small, and cell-cell interactions are negligible. Hence, the primary force acting on the platelets is the secondary Dean drag force which carries them to the outer section of the spiral microchannel through the middle passway.

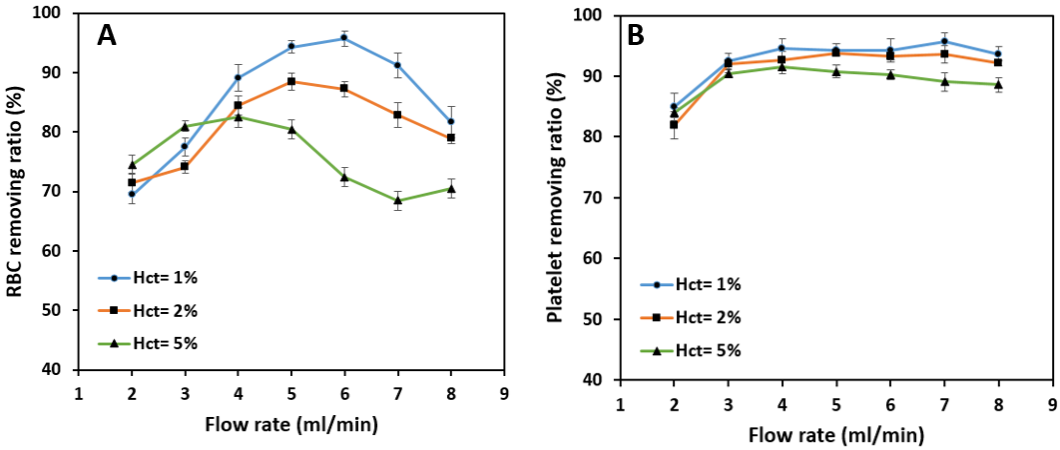

Figure 9. The effect of blood hematocrit on the removing ratio of A) RBC, B) Platelets. Removing ratio mainly decreases with an increase in blood hematocrit due to a rise in the effect of cell-cell interaction. While RBC removing ratio is highly dependent on blood hematocrit, the removing ratio of platelets does not seem to change very much with a change in blood hematocrit.

According to Figure 10A, the overall isolation efficiency of WBCs decreases as hematocrit increases. The efficiency starts at relatively high amounts at the flow rate of 2 ml/min; i.e., 92% and 90.2% for 2% and 5% hematocrits which are lower than 95.2% efficiency value reached by 1% blood hematocrit.

As the flow rate increases, the reduction in isolation efficiency becomes noticeable for higher hematocrits. In terms of purity, higher sample hematocrits are less pure than the sample with 1% hematocrit due to the fact that more RBCs and platelets are present in these samples. The WBC outlet sample has a maximum purity of 78.8% at 6 ml/min and

Preprints (www.preprints.org) | NOT PEER-REVIEWED | Posted: 29 September 2021 doi:10.20944/preprints202109.0482.v1

65.5% at 5 ml/min flow rate for 2% and 5% hematocrits, respectively. These figures are pretty much lower than the maximum purity for 1% hematocrit which is 88.3%. Therefore, increasing the sample hematocrit has a negative effect on WBC purity.

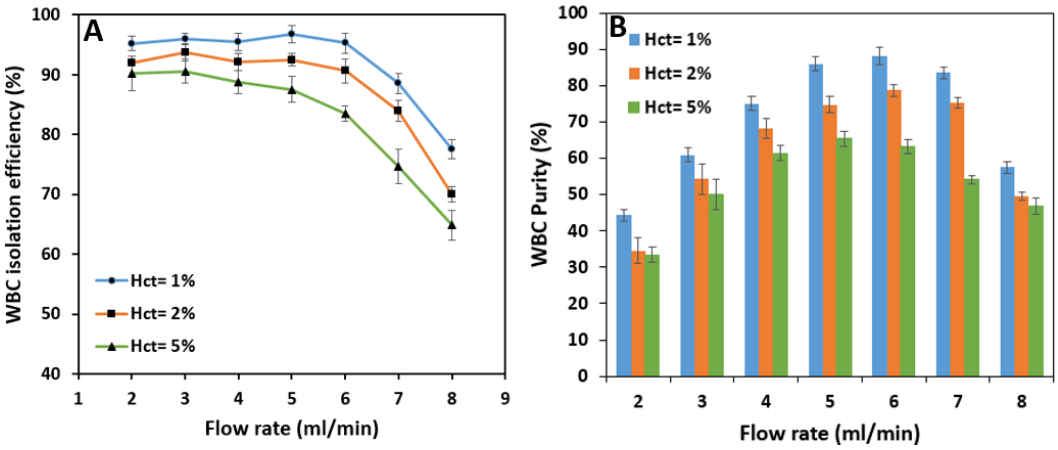

Figure 10. The effect of blood hematocrit on WBCs': A) isolation efficiency, B) purity. Separation efficiency mainly decreases with an increase in blood hematocrit due to a rise in the effect of cell-cell interaction in higher flow rates. Sample purities for lower hematocrits are mainly higher to the lower amount of RBCs in the diluted sample. WBC purity is higher in flow rates of 5,6, and 7 ml/min due to an increase in RBCs removing ratio.

The best overall performances of the spiral microchannel tested at different flow rates and hematocrits are listed and summarized in Table .

Table 1. Summary of the spiral microchip best performance results in the isolation of WBC, RBC, and Platelets

		Sample hematocrit		
		1%	2%	5%
	Flow rate (ml/min)	6	5	4
WBC	Purity (%)	88.3	74.8	61.5
	Isolation efficiency (%)	95.3	92.5	88.8
RBC	Removing ratio (%)	95.7	88.4	82.5
Platelets	Removing ratio (%)	94.2	93.8	91.6

With all things considered, optimum results are achieved under a flow rate of 6 ml/min for a 1% hematocrit blood sample. The illustration of flow and collected blood samples from the microchip outlets are shown in **Error! Reference source not found.**.

Preprints (www.preprints.org) | NOT PEER-REVIEWED | Posted: 29 September 2021 doi:10.20944/preprints202109.0482.v1

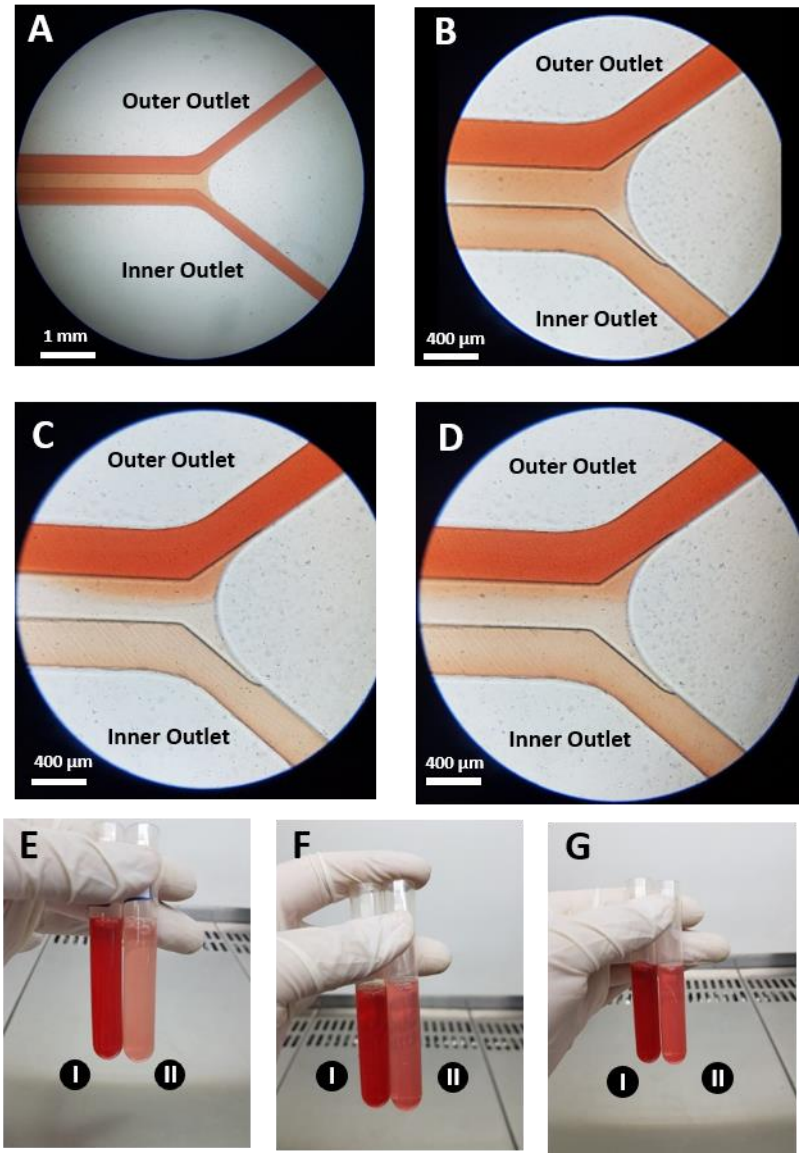

Figure 11. Schematic illustration of the flow in outlet bifurcation in the left spiral microchannel for 1% hematocrit blood sample with A) 2 ml/min B) 4 ml/min C) 6 ml/min and D) 7 ml/min flow rates and collected blood samples with E) 1%, F) 2% and G) 5% hematocrit for 6 ml/min flow rate from microchip: I) outer and II) inner outlets. As can be seen, for constant sample hematocrit, increasing the flow rate reduces the concentration of RBC in the inner outlets, which results in the increases of the WBC and RBC isolation efficiency. For constant flow rates, reducing the sample hematocrit (i.e. higher dilution factors) further reduces the concentration of RBC in the inner outlets, which the collected sample from the inner outlet looks more transparent in comparison to higher sample hematocrits.

The isolation of white blood cells from whole blood has been the main purpose of our spiral microchip. Since the isolation of red blood cells is highly sensitive to inlet flow rates, even a slight improvement in removing the red blood cells from the target outlet is a success. Because any sample contains numerous RBCs compared to other blood components (about 1 WBC to every 600 RBC), we managed to select the best performance based on the best RBC removing ratio. Yet, we had to sacrifice a small amount of WBC efficiency.

The numerical simulations showed that a 5 ml/min flow rate could force particles smaller than 10 µm to migrate to the outer microchannel section while holding the particles larger than 10 µm in the inner section. Although the simulation settings are for the case of a single solid particle dispersed in a Newtonian fluid without the interference of other particles, the experimental reported results are reasonably acceptable for 1% hematocrit at 5-6 ml/min flow rate.

5. Conclusion

This paper proposed a passive cell separating method using two parallel U-shaped spiral microchannels for size-based, label-free and continuous separation of blood cells from whole blood based on cell inertial migration. The U-shaped cross-section spiral microchannel increases cell isolation efficiency by avoiding the re-circulation of smaller cells (RBCs and platelets) through the entire microchip, thus eliminating the major drawback of the conventional rectangular spiral microchannel. Numerical simulations were performed to study the flow behavior, secondary flow distribution, and particle migration mechanism in the proposed design. An algorithm was developed to calculate the hydrodynamic forces exerted on particles present in the U-shaped spiral microchannel to further predict the design's performance before proceeding to the fabrication of the microchip. Subsequently, we successfully isolated different types of blood cells from whole blood in our experiments and investigated the effect of flow rate and hematocrit on the isolation efficiency. The best performance can be achieved for 6 ml/min flow rate with 90.3%, 90.7%, and 92.7% isolation efficiency for WBCs, RBCs, and platelets, respectively, for a 1% hematocrit whole blood sample. The proposed spiral microchip allows a high-throughput, high-efficiency, non-invasive, size-based label-free blood cell separation from whole blood without the assistance of RBC lysis, density gradient centrifugation, cell biomarkers, and chemical treatments on the sample. Most importantly, it can be integrated into more complex microfluidic platforms.

Moreover, we successfully tested the double parallel spiral microchannel. We reached decent isolation results that are already superior to most of the microfluidic cell sorting platforms in case of fast processing time. There is still room for improvement in microchip throughput, which can be done by parallelizing more spiral microchannels while maintaining high isolation efficiencies.

Funding: This research received no external funding.

Institutional Review Board Statement: The study was conducted according to the guidelines of the Declaration of Helsinki and approved by the Research Ethics Committees of Iran University of Medical Sciences (ID: IR.IUMS.REC.1400.285).

Informed Consent Statement: Informed consent was obtained from all subjects involved in the study.

Data Availability Statement: The datasets used and/or analyzed during the current study are available from the corresponding author on reasonable request.

Conflicts of Interest: The authors declare no conflict of interest.

References

1. Kumar, D.; Jain, N.; Khurana, A.; Mittal, S.; Satapathy, S.C.; Senkerik, R.; Hemanth, J.D. Automatic Detection of White Blood Cancer From Bone Marrow Microscopic Images Using Convolutional Neural Networks. *IEEE Access* **2020**, *8*, 142521-142531, doi:10.1109/ACCESS.2020.3012292.
2. Braun, D.P.; Harris, J.E. Relationship of Leukocyte Numbers, Immunoregulatory Cell Function, and Phytohemagglutinin Responsiveness in Cancer Patients23. *JNCI: Journal of the National Cancer Institute* **1981**, *67*, 809-814, doi:10.1093/jnci/67.4.809.
3. Nairn, J.; Hodge, G.; Henning, P. Changes in leukocyte subsets: clinical implications for children with chronic renal failure. *Pediatr Nephrol* **2005**, *20*, 190-196, doi:10.1007/s00467-004-1727-2.
4. Gossett, D.R.; Weaver, W.M.; Mach, A.J.; Hur, S.C.; Tse, H.T.; Lee, W.; Amini, H.; Di Carlo, D. Label-free cell separation and sorting in microfluidic systems. *Anal Bioanal Chem* **2010**, *397*, 3249-3267, doi:10.1007/s00216-010-3721-9.
5. Rostami, P.; Kashaninejad, N.; Moshksayan, K.; Saidi, M.S.; Firoozabadi, B.; Nguyen, N.-T. Novel approaches in cancer management with circulating tumor cell clusters. *Journal of Science: Advanced Materials and Devices* **2019**, *4*, 1-18, doi:10.1016/j.jsamd.2019.01.006.

6. Tajik, P.; Saidi, M.S.; Kashaninejad, N.; Nguyen, N.-T. Simple, Cost-Effective, and Continuous 3D Dielectrophoretic Microchip for Concentration and Separation of Bioparticles. *Industrial & Engineering Chemistry Research* **2020**, *59*, 3772-3783, doi:10.1021/acs.iecr.9b00771.
7. Lee, G.-H.; Kim, S.-H.; Ahn, K.; Lee, S.-H.; Park, J.Y. Separation and sorting of cells in microsystems using physical principles. *Journal of Micromechanics and Microengineering* **2015**, *26*, 013003, doi:10.1088/0960-1317/26/1/013003.
8. Jeon, H.; Kim, Y.; Lim, G. Continuous particle separation using pressure-driven flow-induced miniaturizing free-flow electrophoresis (PDF-induced μ-FFE). *Scientific Reports* **2016**, *6*, 19911, doi:10.1038/srep19911.
9. Kang, J.H.; Krause, S.; Tobin, H.; Mammoto, A.; Kanapathipillai, M.; Ingber, D.E. A combined micromagnetic-microfluidic device for rapid capture and culture of rare circulating tumor cells. *Lab on a Chip* **2012**, *12*, 2175-2181, doi:10.1039/C2LC40072C.
10. Moon, H.-S.; Kwon, K.; Kim, S.-I.; Han, H.; Sohn, J.; Lee, S.; Jung, H.-I. Continuous separation of breast cancer cells from blood samples using multi-orifice flow fractionation (MOFF) and dielectrophoresis (DEP). *Lab on a Chip* **2011**, *11*, 1118-1125, doi:10.1039/C0LC00345J.
11. Evander, M.; Johansson, L.; Lilliehorn, T.; Piskur, J.; Lindvall, M.; Johansson, S.; Almqvist, M.; Laurell, T.; Nilsson, J. Noninvasive Acoustic Cell Trapping in a Microfluidic Perfusion System for Online Bioassays. *Analytical Chemistry* **2007**, *79*, 2984-2991, doi:10.1021/ac061576v.
12. Hejazian, M.; Li, W.; Nguyen, N.T. Lab on a chip for continuous-flow magnetic cell separation. *Lab Chip* **2015**, *15*, 959-970, doi:10.1039/c4lc01422g.
13. McGrath, J.; Jimenez, M.; Bridle, H. Deterministic lateral displacement for particle separation: a review. *Lab on a Chip* **2014**, *14*, 4139-4158, doi:10.1039/C4LC00939H.
14. Yamada, M.; Nakashima, M.; Seki, M. Pinched Flow Fractionation: Continuous Size Separation of Particles Utilizing a Laminar Flow Profile in a Pinched Microchannel. *Analytical Chemistry* **2004**, *76*, 5465-5471, doi:10.1021/ac049863r.
15. Oakey, J.; Allely, J.; Marr, D.W.M. Laminar-Flow-Based Separations at the Microscale. *Biotechnology Progress* **2002**, *18*, 1439-1442, doi:10.1021/bp0256216.
16. Di Carlo, D.; Irimia, D.; Tompkins, R.G.; Toner, M. Continuous inertial focusing, ordering, and separation of particles in microchannels. *Proceedings of the National Academy of Sciences* **2007**, *104*, 18892, doi:10.1073/pnas.0704958104.
17. Sugiyama, D.; Teshima, Y.; Yamanaka, K.; Briones-Nagata, M.P.; Maeki, M.; Yamashita, K.; Takahashi, M.; Miyazaki, M. Simple density-based particle separation in a microfluidic chip. *Analytical Methods* **2014**, *6*, 308-311, doi:10.1039/C3AY40971F.
18. Yoon, Y.; Kim, S.; Lee, J.; Choi, J.; Kim, R.K.; Lee, S.J.; Sul, O.; Lee, S.B. Clogging-free microfluidics for continuous size-based separation of microparticles. *Sci Rep* **2016**, *6*, 26531, doi:10.1038/srep26531.
19. Holmes, D.; Whyte, G.; Bailey, J.; Vergara-Irigaray, N.; Ekpenyong, A.; Guck, J.; Duke, T. Separation of blood cells with differing deformability using deterministic lateral displacement†. *Interface Focus* **2014**, *4*, 20140011, doi:10.1098/rsfs.2014.0011.
20. Segré, G.; Silberberg, A. Radial Particle Displacements in Poiseuille Flow of Suspensions. *Nature* **1961**, *189*, 209-210, doi:10.1038/189209a0.
21. Segré, G.; Silberberg, A. Behaviour of macroscopic rigid spheres in Poiseuille flow Part 1. Determination of local concentration by statistical analysis of particle passages through crossed light beams. *Journal of Fluid Mechanics* **1962**, *14*, 115-135, doi:10.1017/S002211206200110X.
22. Vasseur, P.; Cox, R.G. The lateral migration of a spherical particle in two-dimensional shear flows. *Journal of Fluid Mechanics* **1976**, *78*, 385-413, doi:10.1017/S0022112076002498.
23. Feuillebois, F. Some theoretical results for the motion of solid spherical particles in a viscous fluid. *Multiphase Science and Technology* **1989**, *4*, 583-789, doi:10.1615/MultScienTechn.v4.i1-4.50.

24. Dijkshoorn, J.P.; Schutyser, M.A.I.; Wagterveld, R.M.; Schroën, C.G.P.H.; Boom, R.M. A comparison of microfiltration and inertia-based microfluidics for large scale suspension separation. *Separation and Purification Technology* **2017**, *173*, 86-92, doi:10.1016/j.seppur.2016.09.018.
25. Chun, B.; Ladd, A.J.C. Inertial migration of neutrally buoyant particles in a square duct: An investigation of multiple equilibrium positions. *Physics of Fluids* **2006**, *18*, 031704, doi:10.1063/1.2176587.
26. Kim, Y.W.; Yoo, J.Y. The lateral migration of neutrally-buoyant spheres transported through square microchannels. *Journal of Micromechanics and Microengineering* **2008**, *18*, 065015, doi:10.1088/0960-1317/18/6/065015.
27. Bhagat, A.A.S.; Kuntaegowdanahalli, S.S.; Papautsky, I. Enhanced particle filtration in straight microchannels using shear-modulated inertial migration. *Physics of Fluids* **2008**, *20*, 101702, doi:10.1063/1.2998844.
28. Bhagat, A.A.S.; Kuntaegowdanahalli, S.S.; Papautsky, I. Continuous particle separation in spiral microchannels using dean flows and differential migration. *Lab on a Chip* **2008**, *8*, 1906-1914, doi:10.1039/B807107A.
29. Warkiani, M.E.; Khoo, B.L.; Wu, L.; Tay, A.K.P.; Bhagat, A.A.S.; Han, J.; Lim, C.T. Ultra-fast, label-free isolation of circulating tumor cells from blood using spiral microfluidics. *Nature Protocols* **2016**, *11*, 134-148, doi:10.1038/nprot.2016.003.
30. Rafeie, M.; Zhang, J.; Asadnia, M.; Li, W.; Warkiani, M.E. Multiplexing slanted spiral microchannels for ultra-fast blood plasma separation. *Lab on a Chip* **2016**, *16*, 2791-2802, doi:10.1039/C6LC00713A.
31. Di Carlo, D.; Edd, J.F.; Humphry, K.J.; Stone, H.A.; Toner, M. Particle Segregation and Dynamics in Confined Flows. *Physical Review Letters* **2009**, *102*, 094503, doi:10.1103/PhysRevLett.102.094503.
32. Martel, J.M. Particle Focusing in Microchannels. Doctoral dissertation, Harvard University, 2014.
33. Sun, J.; Li, M.; Liu, C.; Zhang, Y.; Liu, D.; Liu, W.; Hu, G.; Jiang, X. Double spiral microchannel for label-free tumor cell separation and enrichment. *Lab on a Chip* **2012**, *12*, 3952-3960, doi:10.1039/C2LC40679A.
34. Guan, G.; Wu, L.; Bhagat, A.A.; Li, Z.; Chen, P.C.Y.; Chao, S.; Ong, C.J.; Han, J. Spiral microchannel with rectangular and trapezoidal cross-sections for size based particle separation. *Scientific Reports* **2013**, *3*, 1475, doi:10.1038/srep01475.
35. Syed, M.S.; Marquis, C.; Taylor, R.; Warkiani, M.E. A two-step microengineered system for high-density cell retention from bioreactors. *Separation and Purification Technology* **2021**, *254*, 117610, doi:10.1016/j.seppur.2020.117610.
36. Shen, S.; Tian, C.; Li, T.; Xu, J.; Chen, S.-W.; Tu, Q.; Yuan, M.-S.; Liu, W.; Wang, J. Spiral microchannel with ordered micro-obstacles for continuous and highly-efficient particle separation. *Lab on a Chip* **2017**, *17*, 3578-3591, doi:10.1039/C7LC00691H.
37. Ghadami, S.; Kowsari-Esfahan, R.; Saidi, M.S.; Firoozbakhsh, K. Spiral microchannel with stair-like cross section for size-based particle separation. *Microfluidics and Nanofluidics* **2017**, *21*, 115, doi:10.1007/s10404-017-1950-3.
38. Di Carlo, D. Inertial microfluidics. *Lab on a Chip* **2009**, *9*, 3038-3046, doi:10.1039/B912547G.
39. Matas, J.-P.; Morris, J.F.; Guazzelli, É. Inertial migration of rigid spherical particles in Poiseuille flow. *Journal of Fluid Mechanics* **2004**, *515*, 171-195, doi:10.1017/S0022112004000254.
40. Matas, J.-P.; Morris, J.; Guazzelli, E. Lateral Forces on a Sphere. *Oil & Gas Science and Technology* **2004**, *59*, 59, doi:10.2516/ogst:2004006.
41. Asmolov, E.S. The inertial lift on a spherical particle in a plane Poiseuille flow at large channel Reynolds number. *Journal of Fluid Mechanics* **1999**, *381*, 63-87, doi:10.1017/S0022112098003474.
42. Dean, W.R. XVI. Note on the motion of fluid in a curved pipe. *The London, Edinburgh, and Dublin Philosophical Magazine and Journal of Science* **1927**, *4*, 208-223, doi:10.1080/14786440708564324.
43. Dean, W.R. The streamline motion of fluid in a curved pipe. *Phil. Mag.* **1928**, *5*, 673-693.
44. Ookawara, S.; Higashi, R.; Street, D.; Ogawa, K. Feasibility study on concentration of slurry and classification of contained particles by microchannel. *Chemical Engineering Journal* **2004**, *101*, 171-178, doi:10.1016/j.cej.2003.11.008.
45. Ookawara, S.; Street, D.; Ogawa, K. Numerical study on development of particle concentration profiles in a curved microchannel. *Chemical Engineering Science* **2006**, *61*, 3714-3724, doi:10.1016/j.ces.2006.01.016.

46. Barisam, M.; Saidi, M.S.; Kashaninejad, N.; Vadivelu, R.; Nguyen, N.-T. Numerical Simulation of the Behavior of Toroidal and Spheroidal Multicellular Aggregates in Microfluidic Devices with Microwell and U-Shaped Barrier. *Micromachines* **2017**, *8*, 358.

47. Sheidaei, Z.; Akbarzadeh, P.; Kashaninejad, N. Advances in numerical approaches for microfluidic cell analysis platforms. *Journal of Science: Advanced Materials and Devices* **2020**, *5*, 295-307, doi:10.1016/j.jsamd.2020.07.008.